# Efficient Vocabulary-Free Fine-Grained Visual Recognition in the Age of Multimodal LLMs

# Hari Chandana Kuchibhotla <sup>1</sup> Sai Srinivas Kancheti <sup>1</sup> Abbavaram Gowtham Reddy <sup>2</sup> Vineeth N Balasubramanian <sup>1</sup>

#### **Abstract**

Fine-grained Visual Recognition (FGVR) involves distinguishing between visually similar categories, which is inherently challenging due to subtle inter-class differences and the need for large, expert-annotated datasets. In domains like medical imaging, such curated datasets are unavailable due to issues like privacy concerns and high annotation costs. In such scenarios lacking labeled data, an FGVR model cannot rely on a predefined set of training labels, and hence has an unconstrained output space for predictions. We refer to this task as Vocabulary-Free FGVR (VF-FGVR), where a model must predict labels from an unconstrained output space without prior label information. While recent Multimodal Large Language Models (MLLMs) show potential for VF-FGVR, querying these models for each test input is impractical because of high costs and prohibitive inference times. To address these limitations, we introduce Nearest-Neighbor Label **R**efinement (NeaR), a novel approach that finetunes a downstream CLIP model using labels generated by an MLLM. Our approach constructs a weakly supervised dataset from a small, unlabeled training set, leveraging MLLMs for label generation. NeaR is designed to handle the noise, stochasticity, and open-endedness inherent in labels generated by MLLMs, and establishes a new benchmark for efficient VF-FGVR.

#### 1. Introduction

Fine-Grained Visual Recognition (FGVR) is a task in computer vision that focuses on distinguishing between highly similar categories within a broader class (Wei et al., 2021). This task has gained increased importance in recent years given the success of foundation models on coarse-grained classification tasks. Traditional image classification aims

Method	Training Time	Inference Time	Cost (\$)	cACC
FineR (Liu et al., 2024a)	10 h	1.12 h	0	57.0
† GPT-40	-	17.5 h	$\sim 100$	59.2
ZS-CLIP + GPT-4o	-	0.03 h	1	54.6
NeaR + GPT-4o (Ours)	$1.57 \ h$	0.03 h	1	67.6
‡ LLaMA	-	9.12 h	0	48.4
ZS-CLIP + LLaMA	-	$0.03 \ h$	0	60.5
NeaR + LLaMA (Ours)	1.57 h	$0.03 \ h$	0	65.0

Table 1: Performance and cost metrics for different methods on benchmark FGVR datasets (computed over 32,503 images from the test sets).  $\dagger$  = proprietary models,  $\ddagger$  = open-source models (both used only for inference). Our method NeaR achieves a clustering accuracy (cACC described in § 4) that exceeds even direct MLLM queries, at a fraction of cost and time taken.

to differentiate between dogs, cats, and birds, while FGVR aims to distinguish between different subcategories, such as *Tennessee Warbler*, *Yellow-rumped Warbler* and *Orange-crowned Warbler* among birds as an example. Fine-grained understanding is essential for a wide range of applications including biodiversity studies (Liu et al., 2024b; Yang et al., 2020), medical diagnosis (Ridzuan et al., 2022; Sohoni et al., 2020), manufacturing (Yang et al., 2022), fashion retail (Cheng et al., 2021) and agriculture (Yang et al., 2020).

FGVR poses significant challenges due to the subtle differences between categories and the need for large annotated datasets. Typically, fine-grained classification datasets are annotated by domain experts who meticulously examine each image and assign a corresponding label. However, when such domain experts are unavailable, not only is labeled data unavailable, but the underlying fine-grained categories of interest may also be unknown. We refer to this task as Vocabulary-Free FGVR (VF-FGVR), where the vocabulary of fine-grained labels is not provided. In this context, pre-trained Multimodal Large Language Models (MLLMs), which are trained on vast corpora of image-text data and possess extensive world knowledge, provide a contemporary solution (Reid et al., 2024). MLLMs excel at zeroshot multimodal tasks such as Visual Question Answering (VQA). By recasting FGVR as a VQA problem, where we ask the question 'What is the best fine-grained class label for this image?', MLLMs can predict fine-grained labels in a zero-shot manner without prior training on a specific dataset. The ability of MLLMs to operate

<sup>&</sup>lt;sup>1</sup>Indian Institute of Technology Hyderabad, India <sup>2</sup>CISPA Helmholtz Center for Information Security, Saarbrücken, Germany. Correspondence to: Hari Chandana Kuchibhotla <ai20resch11006@iith.ac.in>.

in a VF setting presents a promising approach for domains where curated, labeled datasets are scarce or unavailable. However, querying such large models for each test input is computationally expensive and time-consuming, making their usage impractical at scale. As shown in Table 1, performing inference with GPT-4o (Achiam et al., 2023) on 32,203 test images from benchmark FGVR datasets takes  $\approx 17.5$  hours of querying and incurs a cost of  $\approx$  USD \$100.

Hence, especially considering the need for sustainable AI systems, there is an imminent need for an efficient VF-FGVR system that performs on par with MLLMs on the fine-grained understanding task, while being efficient in terms of time and computational resources required. We focus on this problem in this work. To this end, we only consider access to a small unlabeled set of training images belonging to the classes of interest, with no information regarding the individual class names or even the total number of classes. Such unlabeled datasets are relatively easy to obtain for many domains - for instance, a collection of unlabeled photos of exotic birds. We empirically show in § 4 that having about 3 images per class is sufficient to learn an FGVR system that can perform inference for any number of test samples in the considered experiments. To solve this VF-FGVR task, we propose to label this training set by querying an MLLM for each image. Such a noisily labeled training set can be used in different ways - a simple strategy would be to utilize this MLLM supervision to build a zero-shot classifier over the set of generated labels using a pre-trained CLIP (Radford et al., 2021) model. Another way would be to naively fine-tune the CLIP model using the generated labels. In both these approaches, test images can now be classified by the CLIP model without the need for expensive forward passes through an MLLM. Although such simple methods are efficient in compute and time taken, they fall short on performance as shown in § 4. This is because MLLM outputs are inherently noisy and open-ended, so the generated labels do not necessarily provide strong supervision.

To address these limitations, we propose Nearest-Neighbor Label Refinement (NeaR), a method designed to learn using the noisy labels generated by an MLLM. Our approach first constructs a candidate label set for each image using the generated labels of other similar images. In line with prior work on learning with noisy labels (LNL) (Li et al., 2020), we partition the dataset into clean and noisy samples. We then design a label refinement scheme for both partitions that can effectively combine information from the constructed candidate set and the generated label. Finally, to address the open-ended nature of MLLM outputs, we incorporate a label filtering mechanism to truncate the label space. Our method NeaR thus enables us to handle the inherently noisy and open-ended labels generated by MLLMs, allowing us to effectively fine-tune a downstream CLIP model. As shown in Table 1, for GPT-40, our approach can achieve performance exceeding that of direct inference while incurring only  $1/100^{th}$  of the total inference cost, and requiring a negligible fraction of inference time.

Our key contributions can be summarized as: (i) To the best of our knowledge, this is the first work that uses state-of-the-art MLLMs to build a cost-efficient vocabulary-free fine-grained visual recognition system, (ii) We propose a pipeline that can handle noisy and open-ended labels generated by an MLLM. Our proposed method NeaR leverages similarity information to construct a candidate label set for each image which is used to mitigate the impact of label noise. We also design a label filtering mechanism to improve classification performance. (iii) We perform a comprehensive set of experiments showing that NeaR outperforms existing works and the MLLM-based baselines we introduce for VF-FGVR, achieving this in a cost-efficient way.

#### 2. Related Work

Fine-Grained Visual Recognition. FGVR (Wah et al., 2011; Maji et al., 2013) aims to identify sub categories of an object, such as various bird species, aircraft type etc. FGVR has been extensively studied in prior work (Wei et al., 2021). A key limitation of these methods is their reliance on annotated datasets, which are often unavailable in many important domains like e-commerce and medical data. With advancements in Vision-Language Models and MLLMs, the burden of dataset annotation can be alleviated, reducing the need for extensive human effort. **Foundation** Models for VF-FGVR. Recent advancements in MLLMs have led to models demonstrating strong zero-shot performance across a wide range of multimodal tasks (Li et al., 2023; Achiam et al., 2023; Reid et al., 2024; Touvron et al., 2023; Liu et al., 2023). These MLLMs can be applied to VF-FGVR by framing the task as a VQA problem. MLLMs are broadly categorized into two types: (1) Proprietary models, such as GPT-40 (Achiam et al., 2023) and GeminiPro (Reid et al., 2024), and (2) Open-source models, including BLIP-v2 (Li et al., 2023), LLaVA-1.5-7B (Liu et al., 2023), LLaMA-3.2-11B (Touvron et al., 2023) and Owen2-7B (Wang et al., 2024). As shown in Table 1, for both types of MLLMs, performing inference for every test point remains computationally expensive and time-consuming. To address this, recent works have developed more efficient solutions for VF-FGVR. For instance, (Liu et al., 2024a;c; Conti et al., 2023) propose pipelines that use cascades of MLLMs. FineR (Liu et al., 2024a) presents a pipeline combining VQA systems, Large Language Models (LLMs), and a downstream CLIP model, leveraging unsupervised data to build a multimodal classifier for inference. RAR (Liu et al., 2024c) uses a multimodal retriever with external memory, retrieving and ranking top-k samples using an LLM. CaSED (Conti et al., 2023) approaches VF-FGVR by accessing an

external database to retrieve relevant text for a given image. Nevertheless, these methods are often complex and do not fully exploit the advancements in MLLMs, resulting in suboptimal performance. **Prompt Tuning.** Prompt-tuning methods add a small number of learnable tokens to the input while keeping the pretrained parameters unchanged. The tokens are fine-tuned to enhance the performance of large pre-trained models on specific tasks. Context Optimization (CoOp) (Zhou et al., 2021) was the first to introduce textbased prompt tuning, replacing manually designed prompts like "a photo of a" with adaptive soft prompts. We study the impact of our method under other prompt-tuning methods such as VPT (Jia et al., 2022) and IVLP (Rasheed et al., 2022) in Appendix A7.2. Learning with Noisy Labels. (Arpit et al., 2017) demonstrated the memorization effect of deep networks, showing that models tend to learn clean patterns before fitting noisy labels. To mitigate this, (Han et al., 2018; Chen et al., 2019) introduce iterative learning methods to filter out noisy samples during training. (Arazo et al., 2019) proposed a mixture model-based approach to partition datasets into clean and noisy subsets, leading to more reliable training. Building on these insights, DivideMix (Li et al., 2020), a state-of-the-art LNL method, combines semisupervised learning with data partitioning to achieve superior performance on noisy datasets. JoAPR (Guo & Gu, 2024) is a contemporary approach to fine-tune CLIP on noisy few-shot data. We compare against JoAPR in § 4.

#### 3. Methodology

As shown in Table 1, although MLLMs are capable of performing VF-FGVR, labeling every test image is expensive and time consuming which limits their practical application. To address these limitations, we propose **Nea**rest-Neighbor Label Refinement (NeaR), a method designed to leverage MLLMs efficiently for VF-FGVR. Our approach begins by constructing a candidate label set for each unlabeled training image as described in § 3.2. Next we partition the data into 'clean' and 'noisy' samples using a Gaussian Mixture Model (GMM) and the small-loss rule (Arpit et al., 2017). In § 3.3, we show how to refine labels of noisy samples by incorporating information from the candidate sets. The final loss function is a simple cross-entropy loss, where the refined labels serve as the targets. As outlined in § 3.1, using MLLM outputs directly can result in an excessively large label space, which can hinder performance. To address this, NeaR incorporates a label filtering mechanism to truncate the label space, which boosts classification performance while improving efficiency. Once the CLIP model is fine-tuned, it can classify test images without requiring additional expensive forward passes through an MLLM, significantly improving inference efficiency. Our methodology NeaR is able to exceed the performance of direct MLLMbased classification at just a fraction of the cost and compute. An overview of our methodology is presented in Figure 1, and the pseudocode is detailed in Algorithm§ 1 in the appendix. We begin by discussing the necessary preliminaries.

#### 3.1. Preliminaries

**Problem Formalization.** We consider a setting where only a small, unlabeled training set of n images  $X = \{x_i\}_{i=1}^n$ ,  $x_i \in \mathcal{X}$  is available. We assume that this training set has at least m-shot samples for each class of the unknown ground-truth class name set  $\mathcal{G}$ . We also study a more realistic scenario where there is class imbalance in § 4.2 and observe that the performance of NeaR does not degrade. Note that no further information about  $\mathcal{G}$  is known, including its cardinality. For each image  $x_i$ , we obtain a class name  $l_i = L(x_i, p)$  from an MLLM L, where p is a simple text prompt 'Provide a best fine-grained class name for this image.' that guides the MLLM to generate a fine-grained class name for the image. The generated dataset  $\mathcal{D} = \{(x_i, l_i)\}_{i=1}^n$  consists of n image-label pairs, and the output space of class names is denoted by  $\mathcal{C} = \bigcup_{i=1}^n l_i$ . W.l.o.g. we assume  $\mathcal{C}$  is lexicographically ordered and we denote the  $k = |\mathcal{C}|$  labels by  $C = \{c_1, c_2, \dots, c_k\}$ . Let  $y_i \in \{0, 1\}^k$ ,  $i \in [n]$ , denote the one-hot encoding of the text label  $l_i$  for image  $x_i$  i.e  $y_i^j = 1$  if  $l_i = c_j$  and 0 otherwise. Due to the inherent noise and stochastic nature of MLLM generated labels, it is common to have  $|\mathcal{C}| > |\mathcal{G}|$ . Furthermore, the number of generated labels increases with the size of the training set and can become prohibitively large, hampering training and reducing efficiency of the downstream CLIP classifier.

**CLIP Classifier:** CLIP (Radford et al., 2021) consists of an image encoder  $\mathcal{I}$  and a text encoder  $\mathcal{T}$  trained contrastively on image-text pairs. For VF-FGVR, we first query an MLLM to build a few-shot dataset  $\mathcal{D}$  with label space  $\mathcal{C}$ . CLIP classifies image x as  $\hat{l}(x) = \arg\max_{l \in \mathcal{C}} \cos(\mathcal{I}(x), \mathcal{T}(l))$ . We call this baseline ZS-CLIP. Note that ZS-CLIP does not leverage the paired supervision in  $\mathcal{D}$  and thus serves as a simple baseline. CLIP can benefit from fine-tuning on a small labeled datast. CoOp (Zhou et al., 2021) is a prompt-tuning approach that adds a small number of learnable tokens  $\theta$  to the class name. We denote CLIP's class predictions by  $f_{\theta}(x) \in \Delta^k$ , where  $\Delta^k$  denotes the k-1 simplex. The prompts are trained on the dataset  $\mathcal{D}$  by minimizing cross-entropy loss

$$L_{CE}(\theta) = \frac{-1}{n} \sum_{i=1}^{n} \sum_{j=1}^{k} y_i^j log(f_{\theta}^j(x_i))$$
. Naive finetuning

using CoOp on a dataset generated by an MLLM can be susceptible to label noise. Our NeaR method mitigates this issue by refining labels through nearest-neighbor information. The following sections detail how NeaR constructs candidate sets, learns with these sets, and filters labels for effective downstream performance.

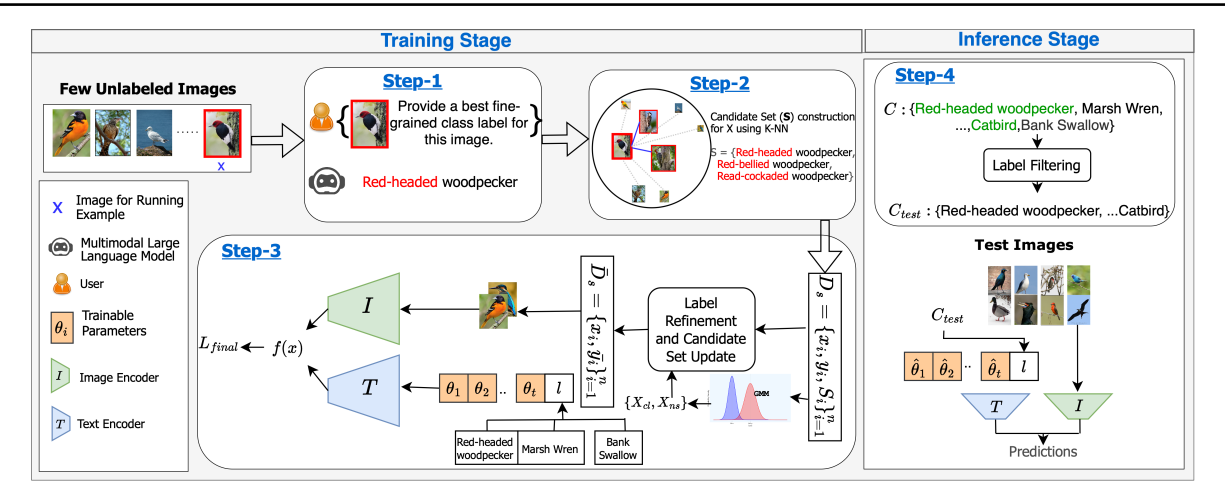


Figure 1: Overview of our proposed method, NeaR, for Vocabulary-Free Fine-Grained Visual Recognition (VF-FGVR). In the Training Stage, we start with a few unlabeled images. Step-1: An MLLM generates a best-estimate fine-grained label (e.g., "Red-headed woodpecker") for each image. Step-2: A candidate label set is constructed using K-Nearest Neighbors, capturing related fine-grained classes. Step-3: The model is fine-tuned using a CLIP-based architecture. A GMM is applied to the loss to partition the data into clean and noisy samples. Based on this split, a label refinement mechanism is used to further update and refine the labels. The final loss,  $L_{final}$ , is then computed, and the model parameters are updated accordingly. In the Inference Stage, we apply label filtering to limit the label space (Step-4). Our approach handles the noise and open-ended nature of MLLM-generated labels, significantly reducing inference time and cost while maintaining performance.

#### 3.2. NeaR: Candidate Set Construction

The label generated by an MLLM in response to a prompt may vary significantly from the ground truth class label for each image. We propose to leverage local geometry to mitigate the noise in generated labels. More formally, we make the manifold assumption, which suggests that similar images should share similar or identical class labels (Iscen et al., 2022; Li et al., 2022). This is particularly useful when the label  $l_i$  assigned to image  $x_i$  by the MLLM is incorrect, which we refer to as a noisy label. By constructing a candidate label set, we increase the likelihood of including the true label or a semantically closer alternative in the candidate set rather than relying solely on the potentially incorrect label provided by the MLLM. Table 2 shows that the semantic similarity between the best label in the candidate set and the ground truth is higher than that of the noisy single label, supporting our hypothesis. We use CLIP's pretrained image encoder  $\mathcal{I}$  to extract image features of the entire training set X. For each image  $x_i$ , we select the top- $\kappa$  most similar images (including  $x_i$  itself) and gather their corresponding labels to form the candidate set  $S_i = (l_i, l_1, \dots, l_{\kappa-1})$ . In this work, we choose  $\kappa = 3$ . The resulting dataset is reconstructed as  $\mathcal{D}_s = \{(x_i, l_i, S_i)\}_{i=1}^n$ , incorporating the candidate sets rather than single labels alone. An alternative way of noise mitigation is to have the MLLM directly generate a candidate set of 'top- $\kappa$ ' labels for each image, instead of just a single label. However this approach does not make use of similarity information between images, as each candidate set is now generated independently, leading to an excessively large label space. We empirically demonstrate

Method	Bird-200	Car-196	Dog-120	Flower-102	Pet-37
MLLM Labels	69.9	78.6	70.9	57.9	84.8
Random CS	72.8	78.9	73.6	61.6	85.9
K-NN CS (ours)	78.0	81.3	75.5	65.8	87.4

Table 2: The table compares the quality of labels generated by the MLLM, Random candidate set (CS), and K-NN CS using sACC. While Random CS modestly increases the likelihood of including the true label compared to using MLLM labels directly, K-NN CS significantly outperforms Random CS, generating a superior candidate set and validating our hypothesis.

the effectiveness of our nearest-neighbor based candidate set generation over other alternatives in Appendix § A7.1.

### 3.3. NeaR: Learning With a Candidate Set

We treat the candidate sets as a source of supplementary similarity information to be used in conjunction with the label. As explained below, for a *noisy* image, where the initial label  $l_i$  is incorrect, we propose relying on the candidate set  $S_i$  to mitigate the impact of noise. Conversely, for a *clean* image, we can trust and utilize its generated label  $l_i$ .

**Detecting Noisy Samples.** It has been demonstrated in (Arpit et al., 2017) that models tend to learn clean samples before noisy ones, resulting in lower loss values for clean samples. Following DivideMix (Li et al., 2020), for every training epoch, we fit a two-component Gaussian Mixture Model (GMM) over the cross entropy loss values of all training samples  $\{L(x_i, l_i)\}_{i=1}^n$ , where  $L(x_i, l_i) = -\sum_{j=1}^k y_i^j log(f_\theta^j(x_i))$ ,  $y_i$  is the one-hot encoding of  $l_i$ . The component with the smaller mean value models the clean samples, while the other component models the noisy ones. The posterior probability  $w_i = \mathbb{P}_{GMM}(clean|x_i)$ 

computed from the fitted GMM is used to model the likelihood that a sample  $x_i$  is clean. This GMM is refitted for every training epoch, enabling dynamic estimation of label noise over time. We now partition the training data into clean  $X_{cl} = \{x_i \in X \mid w_i \geq \tau\}$  and noisy  $X_{ns} = X \setminus X_{cl}$ sets based on clean probability threshold au. We use the average clean posterior as an adaptive threshold for every epoch, i.e  $\tau = \frac{1}{n} \sum_{i=1}^{n} w_i$ . The effect of different thresholding strategies is presented in Appendix § A7.

Warm-up. Warm-up strategies are commonly used to speedup convergence and stabilize training. As demonstrated in (Li et al., 2020), an initial warm-up phase allows the model to learn the clean samples better, resulting in better separation between the losses of clean and noisy samples. During warm-up, we train prompts for a few epochs (10 in our experiments) by minimizing the cross entropy loss over the generated labels  $l_i$  with one-hot representation  $y_i$ :

$$L_{warmup}(\theta) = \frac{-1}{n} \sum_{i=1}^{n} \sum_{j=1}^{k} y_i^j \cdot log(f_{\theta}^j(x_i))$$

This warm-up step lays the groundwork for effective training by allowing the model to initially focus on images labeled correctly by the MLLM.

Candidate Set Guided Label Refinement. Following the initial warm-up phase, we make a forward pass over the entire training set at each training epoch to fit a GMM and partition data into clean and noisy samples  $X_{cl}$  &  $X_{ns}$  as described earlier. We model the confidence of the candidate set  $S_i$  by a vector  $q_i \in \mathbb{R}^k$  for each image  $i \in [n]$ , initialized as  $q_i^j = \frac{1}{|S_i|}$  if  $c_j \in S_i$  and 0 otherwise. This initialization reflects uniform confidence over classes belonging to the candidate set, and zero for non-members.

A candidate set is derived from neighboring images and provides a broader view of possibly correct labels. Our approach constructs refined labels to effectively leverage this additional information. We propose to construct refined labels for clean and noisy images differently. For an image  $x_i$  with one-hot label  $y_i$  and candidate set confidence  $q_i$ , we

$$\bar{y}_i = \begin{cases} \operatorname{shrp}(w_i \cdot y_i + (1 - w_i) \cdot f_{\theta}(x_i), T), & \text{if } x_i \in X_{cl} \\ \operatorname{rsc}(\operatorname{shrp}(w_i \cdot q_i + (1 - w_i) \cdot f_{\theta}(x_i), T), q_i), & \text{o/w} \end{cases}$$

where  $w_i$  is the GMM clean posterior probability, and  $f_{\theta}(x_i)$  denotes the CLIP model class probabilities with learnable prompts  $\theta$ . The sharpen function  $shrp(y,T)^i =$  $(y^i)^{\frac{1}{T}}/\sum_{j=1}^k (y^j)^{\frac{1}{T}}$ , as defined in (Berthelot et al., 2019), adjusts a probability distribution y to be more confident using a temperature T. The rescale function  $rsc(y,q)^i =$  $(y \odot q)^i / \sum_{i=1}^k (y \odot q)^j$  rescales a probability y with the current confidence estimates of the candidate set q. This ensures that the refined label has non-zero probabilities only for the candidate labels. For both clean & noisy images, we update candidate set confidence to be used in the next epoch as  $q_i = \operatorname{rsc}(f_{\theta}(x_i), 1[q_i])$  where  $1[q_i]$  is 1 at non-zero indices. Prompts are learned by minimizing the cross-entropy loss between the refined labels  $\bar{y}$  and CLIP model output.

$$L_{final}(\theta) = \frac{-1}{n} \sum_{i=1}^{n} \sum_{j=1}^{k} \bar{y}_i^j \cdot log(f_{\theta}^j(x_i))$$

Connection to PRODEN. Our loss is similar in spirit to losses designed for Partial Label Learning (PLL), such as PRODEN (Feng et al., 2020), which allow learning when only candidate labels are present. However unlike the PLL setting, our candidate sets are constructed for every image using noisy MLLM outputs, and may not contain the true label. Furthermore, our method uniquely benefits from access to an initial 'best-estimate' label  $l_i$  generated by the MLLM, which is not exploited by traditional PLL algorithms. This best estimate label allows us to differentiate clean samples and helps training convergence by transferring knowledge from clean to noisy samples through iterative updates of q.

#### 3.4. NeaR: Label Filtering

Although we train on the entire label set C, we observe that many labels are noisy and can be removed from the inference time label space. Let  $F_{clip} = \{c_i \mid \exists x \in X \text{ s.t } i = a\}$  $\arg\max f_{\theta}^{j}(x)$ } be a filtered set of labels which are pre-

dicted by CLIP on the training set. Let  $F_{cand} = \{c_i \mid$ s.t  $i = \arg \max q_i^{j}$  be another filtered set of labels which

are predicted using just the candidate sets. We propose to keep only those labels which belong to both sets. The evaluation time label space is  $C_{test} = F_{clip} \cap F_{cand}$  and the inference time prediction of an image x is l(x) = $\arg\max sim(\mathcal{I}(x),\mathcal{T}_{\hat{\theta}}(l))$ , where  $\hat{\theta}$  are the learned prompts.

Label filtering is effective as shown in Table § A9.

#### 4. Experiments and Results

In this section, we comprehensively evaluate the classification performance of NeaR for the VF-FGVR task. We begin by describing the datasets, metrics and benchmark methods we compare against.

Datasets: We perform experiments on five benchmark fine-grained datasets: CaltechUCSD Bird-200 (Wah et al., 2011), Stanford Car-196 (Khosla et al., 2011), Stanford Dog-120 (Krause et al., 2013), Flower-102 (Nilsback & Zisserman, 2008), Oxford-IIIT Pet-37 (Parkhi et al., 2012). Following (Liu et al., 2024a), for each dataset, NeaR and other baselines only have access to m unlabeled training images per class. Unless specified otherwise, we assume m=3. Results for  $1 \le m \le 10$  are shown in Figure 2.

Method	Bird	-200	Car	-196	Dog	-120	Flowe	er-102	Pet	-37	Ave	rage
	cACC	sACC	cACC	sACC	cACC	sACC	cACC	sACC	cACC	sACC	cACC	sACC
ZS-CLIP-GT (Upper Bound)	57.2	80.1	64.0	66.5	60.2	77.6	70.8	79.7	87.5	92.0	68.0	79.2
CaSED	25.6	50.1	26.9	41.4	38.0	55.9	67.2	52.3	60.9	63.6	43.7	52.6
FineR	51.1	69.5	49.2	63.5	48.1	64.9	63.8	51.3	72.9	72.4	57.0	64.3
RAR	51.6	69.5	53.2	63.6	50.0	65.2	63.7	53.2	74.1	74.8	58.5	65.3
†GPT-40	68.8	85.2	37.4	61.5	71.1	80.4	50.5	51.6	68.2	83.5	59.2	72.4
ZS-CLIP-GPT4o	48.8	72.5	42.9	59.5	43.8	69.1	18.2	53.0	68.2	78.7	54.6	66.6
CoOp-GPT-4o	54.4	75.4	51.9	59.8	60.4	72.9	70.4	51.7	83.5	86.3	64.1	69.2
NeaR-GPT4o	55.8	75.6	57.0	60.0	61.6	74.4	80.6	52.1	82.9	84.0	67.6(+3.5%)	69.2
†Gemini Pro	66.1	82.7	35.4	62.8	65.8	81.2	45.3	54.3	71.3	85.7	56.8	73.3
ZS-CLIP-GeminiPro	51.7	74.6	41.6	61.7	58.9	72.6	57.7	49.1	71.7	78.6	56.3	67.3
CoOp-GeminiPro	55.2	75.9	50.2	61.5	62.7	73.8	68.3	51.2	81.6	83.8	63.6	69.2
NeaR-GeminiPro	55.9	76.0	54.9	61.1	64.7	75.4	77.9	53.2	79.4	80.8	66.6(+3%)	69.3(+0.1%)
‡Qwen2-VL-7B-Instruct	53.0	75.3	45.6	63.7	69.7	78.8	84.8	72.7	77.7	85.1	66.2	75.1
ZS-CLIP-Qwen2	41.0	66.0	50.8	60.8	59.3	70.5	66.7	55.2	72.4	77.2	58.0	65.9
CoOp-Qwen2	51.0	72.1	52.1	61.9	62.5	73.4	77.0	65.0	83.4	87.5	65.2	72.0
NeaR-Qwen2	48.9	72.0	55.6	63.2	62.0	73.3	81.4	68.0	84.6	86.8	66.5(+1.3%)	71.7(-0.3%)
‡LLaMA-3.2-11B	41.4	70.6	14.4	61.6	55.0	71.8	66.0	63.6	65.1	82.0	48.4	69.9
ZS-CLIP-LLaMA	48.7	66.3	45.8	60.6	57.4	65.9	74.8	58.4	76.0	78.4	60.5	65.9
CoOp-LLaMA	49.2	68.7	45.5	60.7	58.4	68.4	75.9	59.8	74.4	79.2	60.7	67.4
NeaR-LLaMA	51.0	70.2	52.6	60.9	59.2	70.2	78.6	61.7	83.5	86.2	65.0(+4.3%)	69.8(+2.4%)

Table 3: ZS-Zero Shot,  $\dagger$  proprietary models used for inference,  $\dagger$  open-source models used for inference. Our results shown here are for  $\kappa=3$  and m=3. The first row is ZS-CLIP performance when the ground-truth label space is given, serving as an upper bound. The second partition consists of contemporary VF baselines of which FineR (Liu et al., 2024a) is best performing. We outperform FineR by a large margin, even when using weaker open-source MLLMs. The next four partitions are for labels generated by various MLLMs. We compare NeaR against CoOp within each partition, and highlight best numbers in **bold**. Our method NeaR outperforms all contemporary baselines, as well as ZS-CLIP and CoOp baselines for a variety of MLLMs.

Baselines: We compare our method NeaR against four different classes of baseline methods. Direct Inference on MLLMs. For every test image, we directly query an MLLM for a fine-grained label using a text prompt such as 'What is the best fine-grained class name for this image?'. We evaluate two proprietary MLLMs -GPT-40 (Achiam et al., 2023) and GeminiPro (Reid et al., 2024) and two strong open-source MLLMs, LLaMA-3.2-11B-Vision-Instruct (Touvron et al., 2023) and Qwen2-VL-7B-Instruct (Wang et al., 2024). In the Appendix § A7, we show results on two other weaker open-source MLLMs, BLIP-2 (Li et al., 2023) and LLaVA-1.5 (Liu et al., 2023). (ii) Contemporary VF Baselines. We consider three contemporary baselines which do not require expert annotations but use foundational models to perform VF-FGVR - CaSED (Conti et al., 2023), FineR (Liu et al., 2024a) and RAR (Liu et al., 2024c). (iii) ZS-CLIP with MLLM label space. As described in § 3.1, we can perform zero-shot classification using pre-trained CLIP over the label space generated by querying various MLLMs on training images. We consider four variants of ZS-CLIP - ZS-CLIP-GPT40, ZS-CLIP-GeminiPro, ZS-CLIP-LLaMA, and ZS-CLIP-Qwen2. (iv) Prompt Tuning Baselines. Following CoOp as described in § 3.1, we directly perform prompt-tuning using the labels generated by an MLLM. We consider four variants

 CoOp-GPT4o, CoOp-GeminiPro, CoOp-LLaMA, and CoOp-Qwen2.

**Evaluation Metrics:** In the VF-FGVR setting, NeaR as

well as all other baselines operate in an unconstrained label space, making accuracy an invalid metric since the predicted labels may never exactly match the ground-truth labels. Following (Liu et al., 2024a; Conti et al., 2023), we evaluate performance using two complementary metrics: Clustering Accuracy (cACC) and Semantic Accuracy (sACC). cACC measures the ability of the model to group similar images together. For M test images with groundtruth labels  $y^*$  and predicted labels  $\hat{y}$ , cACC is computed as  $\max_{p \in \mathcal{P}(\hat{\mathcal{Y}})} \frac{1}{M} \sum_{i=1}^{M} \mathbb{1}(y_i^\star = p(\hat{y}_i))$ , where  $\mathcal{P}(\hat{\mathcal{Y}})$  is the set of all permutations of the generated labels. Since cACC disregards the actual label name, it does not measure if the predictions are semantically correct. Despite this limitation, cACC is a strong evaluation metric and is widely used in areas such as GCD (Vaze et al., 2022), where the goal is to assess consistency of predictions rather than exact label semantics. Semantic closeness is captured by sACC, which measures the cosine similarity between Sentence-BERT (Reimers & Gurevych, 2019) embeddings of the predicted and ground-truth labels. As observed in (Liu et al., 2024a), sACC is a more forgiving metric than cACC, because embedding based similarity methods can capture

general semantics even for completely distinct labels. We hence consider cACC as representative of the model's performance, with sACC acting as a sanity check to ensure that the predicted labels remain meaningful.

Implementation Details: We use CLIP ViT-B/16 (Radford et al., 2021) as the VLM, whose image encoder we also use to find the  $\kappa$ -nearest neighbors, with  $\kappa = 3$  by default. The default number of shots is m = 3, and we use the few-shot training splits provided by FineR. For both the CoOp baseline and our method, we introduce 16 trainable context vectors. We use SGD as the optimizer and train for 50 epochs, with 10 warmup epochs. Further implementation details are provided in Appendix § A8.

#### 4.1. Main Results

In this section we compare NeaR against baselines on five fine-grained datasets. In addition to the considered baselines, we benchmark against JoAPR (Guo & Gu, 2024), a state-ofthe-art noisy label learning method designed for CLIP, and against PRODEN (Feng et al., 2020), a widely used partial label learning algorithm.

Benchmarking NeaR Against Baseline Methods: We evaluate NeaR against the four categories of baselines introduced in § 4 – Direct MLLM inference, contemporary VF methods, zero-shot CLIP, and prompt-tuned CLIP. The results are shown in Table 3, with all numbers reported for 3-shot training images. The first partition of the table, ZS-CLIP-GT, is the performance of pre-trained CLIP when provided with the ground-truth label space, serving as an upper bound. Notably, NeaR-GPT-40 achieves an average cACC just -0.4% below this upper bound, demonstrating it's effectiveness. The next partition consists of contemporary methods that can perform VF-FGVR. Out of these, FineR (Liu et al., 2024a) is conceptually closest to ours as it uses a combination of an LLM and a VQA system to construct a training-free CLIP based classifier. We outperform FineR on all datasets by a margin of at least +8% in average cACC, even when using labels from open-source MLLMs. Moreover, as shown in Table 1, NeaR is significantly more efficient in terms of computation time.

The next four partitions in Table 3 report results using labels generated by GPT-40, GeminiPro, LLaMA-3.2 and Qwen2 respectively. Within each partition, we first present results for direct inference with the MLLM, followed by ZS-CLIP, CoOp, and finally NeaR. Across all MLLMs, NeaR performs the best on average cACC, showing gains of at least +3% over the CoOp baseline for GPT-40, GeminiPro and LLaMA-3.2, and a gain of +1.3% over CoOp for Qwen2. Furthermore, we observe a large performance gain for the difficult Car-196 dataset, where NeaR-LLaMA shows a gain of +7.1% in cACC over CoOp-LLaMA. These results highlight that NeaR effectively learns from the imperfect labels generated by MLLMs, leading to robust and efficient

fine-grained classification.

Comparison against PRODEN: Our loss function resembles those used in Partial Label Learning (PLL), such as PRODEN (Feng et al., 2020), which are designed to handle learning with only candidate sets. To study the efficacy of traditional PLL approaches, we replace the traditional cross-entropy loss used in CoOp with PRODEN, and learn prompts using the candidate sets directly. The results are shown in Table 4, where NeaR outperforms PRODEN by a large margin of 4.3% in cACC and 3.2% in sACC. Unlike in traditional PLL where candidate sets are assumed to include the correct label, our candidate sets are generated for each image using noisy MLLM outputs and may not always contain the true label. Also, NeaR uniquely benefits from an initial "best-estimate" label  $l_i$  from the MLLM, which traditional PLL methods do not exploit. As described in § 3.3, this best-estimate label is used to find "clean" images which have a higher probability of being correctly labeled. Knowledge from these clean samples helps resolve the ambiguity in candidate sets, improving performance.

# Comparison against JoAPR (Guo & Gu, 2024), a Contemporary Noisy Label Learning Method for CLIP:

JoAPR is a prompttuning method designed to fine-tune CLIP on noisy fewshot data. In Table 4, we show the results of using JoAPR to

Method	Avei	verage			
	cACC	sACC			
JoAPR-LLaMA	60.4	68.9			
PRODEN	60.6	66.6			
NeaR-LLaMA	65.0	69.8			

NeaR

learn from noisy Table 4: NeaR outperforms JoAPR and generated PRODEN with LLaMA generated labels, labels. Our method showing an improvement of +4.6% and outperforms +4.4% in average cACC respectively.

JoAPR by +4.6% in average cACC, and by +0.9% in average sACC. For JoAPR we use the default configuration suggested in the paper. These gains highlight that generic noisy-label learning methods, which expect structured noise (such as flips) within a closed label set, do not fully address the challenges posed by open-ended MLLM outputs. By incorporating similarity information, performing candidate set guided label refinement, and performing label filtering, NeaR provides a robust solution to the VF-FGVR problem.

#### 4.2. Ablation Studies

In this section we study the impact of each module of NeaR. NeaR leverages common techniques from existing literature on learning with noisy labels. As described in § 3.3, we have a warm-up phase followed by a partition step where we fit a GMM on loss values to partition the data into clean and noisy samples. These two steps are common to many methods that attempt to learn with noisy labels (Arazo et al., 2019; Li et al., 2020; Guo & Gu, 2024), and are not unique to our method. We now study the impact of our novel

Warmup	GMM	Candidate Set	Label filtering	cACC	sACC
✓	/	×	Х	73.9	60.2
✓	✓	✓	×	73.9 75.6 76.9	60.6
✓	✓	×	✓	76.9	60.1
✓	✓	✓	✓	78.6	61.7

Table 5: Ablation study of NeaR demonstrating the effectiveness of our novel components candidate set and label filtering. We report the ablations on Flowers-102 dataset.

additions - candidate set guided label refinement, and label filtering. The results of this study are shown in Tab 5.

Impact of Candidate Set. The candidate label set for an image is used to refine labels of noisy samples. As described in § 3.3, it is also used to aid in label filtering. To study the effect of removal of the candidate set, we refine the labels of the noisy samples as  $\bar{y}_i = \text{shrp}(f_{\theta}(x_i), T)$ , i.e we only used the sharpened CLIP pseudolabel. We also remove the candidate set based filtering  $F_{cand}$ , as defined in § 3.3. Row 3 of Table 5 gives the result of removal of the candidate set. We observe a drop of -1.6% in cACC of the flowers-102 dataset, compared to our NeaR result in Row 4 where all components are present.

Impact of label filtering. The results of Rows 1 & 2 of Table 5 indicate the importance of performing label filtering. The results in Row 1 act as a simple LNL baseline to our method. We observe a drop of -4.6% cACC and -1%sACC for the flowers dataset, from our method in Row 4. This ablation clearly indicates that our components are crucial to learn from noisy MLLM labels. The result of Row 2 studies the impact of removing label filtering in isolation. We observe a drop of -2.9% cACC compared to our method NeaR in Row 4. These ablations confirm that candidate-set guided label refinement and label filtering are integral for performance.

Imbalanced Training Data: We study the realistic scenario of class imbalance in the few-shot training data.

We simulate long-tail distribution where we randomly select small a number of head classes (10 classes

Table 6. We observe

Method	Average					
	cACC	sACC				
FineR	51.9	61.2				
ZS-CLIP-LLaMA	59.7	64.5				
CoOp-LLaMA	60.0	66.5				
NeaR-LLaMA	65.7 (+5.7%)	70.3 (+3.8%)				

for pet-37) which Table 6: Performance for long-tail class have  $4 \le m \le 10$  distribution of training data, where head samples, and the re- classes have  $4 \le m \le 10$  samples maining tail classes and tail classes have m=3 samples. Both NeaR and CoOp retain performance have m=3 samples. On imbalanced data.NeaR outperforms We show results in CoOp by +5.7% in average cAcc.

that there is no degradation in performance for both CoOp and NeaR. Infact, we note slightly better cACC and sACC values for NeaR on account of the slight increase in the training data. The expanded table is in Appendix § A7.

Analysis on Number of Shots m in Training Data: We explore the effect of the number of images used per class, as presented in Figure 2. We consistently use  $\kappa = 3$  for candidate set construction across all shots. For m = 1, our method performs poorly due to excessive label filtering. However, as the number of shots increases, our candidate set is more informative and performance improves markedly. Our proposed method, NeaR, outperforms CoOp for all m > 2, especially at higher shots where there are more noisy labels. We also observe that cACC drops with increasing mdue to increase in the size of the test time label space.

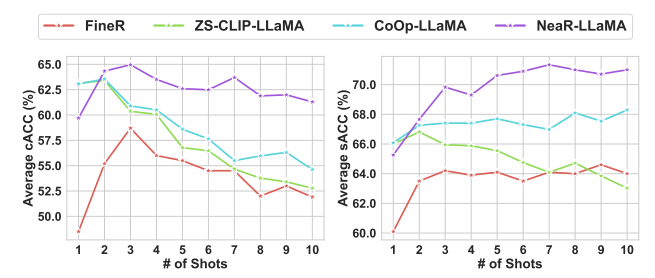


Figure 2: Effect of varying m, number of images per class in training data for labels generated by LLaMA. NeaR (in purple) outperforms CoOp (blue) for all  $m \geq 2$  in average cACC & sACC.

#### Performance of NeaR on Different CLIP Backbones:

All results in this paper are on the ViT-B/16 CLIP backbone. In this section we compare the performance of NeaR-LLaMA with CoOp-LLaMA across vari-

	Method	Avg. cACC	Avg. sACC
RN50	CoOp-LLaMA	18.6	45.0
	NeaR-LLaMA	22.7 (+4.1%)	<b>49.8</b> (+ <b>4.8</b> %)
RN101	CoOp-LLaMA	21.8	45.6
	NeaR-LLaMA	23.6 (+1.8%)	<b>50.5</b> (+ <b>4.9</b> %)
ViT-	CoOp-LLaMA	60.7	67.4
B/16	NeaR-LLaMA	<b>65.0</b> (+4.3%)	69.8 (+2.4%)
ViT-	CoOp-LLaMA	55.7	66.2
B/32	NeaR-LLaMA	<b>61.1</b> (+ <b>5.4</b> %)	68.1 (+1.9%)

ous other CLIP back- Table 7: NeaR outperforms CoOp for difbones. In Table 7 we ferent CLIP backbones using labels genpresent the results of erated by LLaMA for default  $m, \kappa=3$ .

NeaR for a ResNet-50 (He et al., 2015), ResNet-101, and a ViT-B/32 vision-encoder based CLIP model. We use the same configuration for each backbone. NeaR shows consistent improvement, achieving gains of +4.1%, +1.8%, and +5.4% in average cACC for RN50, RN101 and ViT-B/32 respectively. These results highlight the effectiveness of our method over a diverse range of CLIP architectures.

In Appendix § A7 we study different prompting strategies, effect of varying  $\kappa$ , impact of adaptive thresholding, variations across few-shot splits, and show qualitative results.

#### 5. Conclusion

We addressed the challenge of Vocabulary-Free Fine-Grained Visual Recognition (VF-FGVR) by introducing NeaR, a method that leverages MLLMs to generate weakly supervised labels for a small set of training images, to efficiently fine-tune a downstream CLIP model. Our approach constructs a candidate label set for an image using generated

labels of similar images, and performs label refinement for clean and noisy data differently. NeaR also proposes a label filtering strategy, effectively managing the open-ended and noisy nature of MLLM outputs. Experiments on 4 MLLMs show that NeaR significantly outperforms direct inference methods while dramatically reducing computational cost and inference time, setting a new benchmark for efficient and scalable VF-FGVR.

# **Impact Statement**

Our framework relies on MLLM-generated labels, a dependency that is becoming increasingly feasible with advancements in MLLM accessibility. We demonstrate strong performance across both proprietary (GPT-40, GeminiPro) and open-source (LLaMA-11B, Qwen2-7B) models, showing robustness to MLLMs of varying capacities. We see this work as a foundation for future research in leveraging MLLMs for fine-grained recognition, with no direct societal or ethical risks.

#### References

- Achiam, J., Adler, S., Agarwal, S., Ahmad, L., Akkaya, I., Aleman, F. L., Almeida, D., Altenschmidt, J., Altman, S., Anadkat, S., et al. Gpt-4 technical report. *arXiv preprint arXiv:2303.08774*, 2023.
- Arazo, E., Ortego, D., Albert, P., O'Connor, N., and Mcguinness, K. Unsupervised label noise modeling and loss correction. In Chaudhuri, K. and Salakhutdinov, R. (eds.), Proceedings of the 36th International Conference on Machine Learning, volume 97 of Proceedings of Machine Learning Research, pp. 312–321. PMLR, 09–15 Jun 2019.
- Arpit, D., Jastrzebski, S., Ballas, N., Krueger, D., Bengio, E., Kanwal, M. S., Maharaj, T., Fischer, A., Courville, A. C., Bengio, Y., and Lacoste-Julien, S. A closer look at memorization in deep networks. In *International Conference on Machine Learning*, 2017.
- Berthelot, D., Carlini, N., Goodfellow, I. J., Papernot, N., Oliver, A., and Raffel, C. Mixmatch: A holistic approach to semi-supervised learning. *ArXiv*, abs/1905.02249, 2019.
- Chen, P., Liao, B. B., Chen, G., and Zhang, S. Understanding and utilizing deep neural networks trained with noisy labels. In Chaudhuri, K. and Salakhutdinov, R. (eds.), *Proceedings of the 36th International Conference on Machine Learning*, volume 97 of *Proceedings of Machine Learning Research*, pp. 1062–1070. PMLR, 09–15 Jun 2019.
- Cheng, W.-H., Song, S., Chen, C.-Y., Hidayati, S. C., and

- Liu, J. Fashion meets computer vision: A survey. *ACM Computing Surveys*, 54(4), 2021. doi: 10.1145/3447239.
- Conti, A., Fini, E., Mancini, M., Rota, P., Wang, Y., and Ricci, E. Vocabulary-free image classification. *Advances* in Neural Information Processing Systems, 36:30662– 30680, 2023.
- Feng, L., Lv, J., Han, B., Xu, M., Niu, G., Geng, X., An, B., and Sugiyama, M. Provably consistent partial-label learning. In *Proceedings of the 34th International Conference on Neural Information Processing Systems*, NIPS '20, Red Hook, NY, USA, 2020. Curran Associates Inc. ISBN 9781713829546.
- Guo, Y. and Gu, X. Joapr: Cleaning the lens of prompt learning for vision-language models. In *Proceedings* of the IEEE/CVF Conference on Computer Vision and Pattern Recognition, pp. 28695–28705, 2024.
- Han, B., Yao, Q., Yu, X., Niu, G., Xu, M., Hu, W., Tsang, I. W.-H., and Sugiyama, M. Co-teaching: Robust training of deep neural networks with extremely noisy labels. In *Neural Information Processing Systems*, 2018. URL https://api.semanticscholar. org/CorpusID:52065462.
- He, K., Zhang, X., Ren, S., and Sun, J. Deep residual learning for image recognition. 2016 IEEE Conference on Computer Vision and Pattern Recognition (CVPR), pp. 770-778, 2015. URL https://api.semanticscholar.org/CorpusID: 206594692.
- Iscen, A., Valmadre, J., Arnab, A., and Schmid, C. Learning with neighbor consistency for noisy labels. 2022 *IEEE/CVF Conference on Computer Vision and Pattern Recognition (CVPR)*, pp. 4662–4671, 2022.
- Jia, M., Tang, L., Chen, B.-C., Cardie, C., Belongie, S. J., Hariharan, B., and Lim, S. N. Visual prompt tuning. *ArXiv*, abs/2203.12119, 2022.
- Khosla, A., Jayadevaprakash, N., Yao, B., and Li, F.-F. Novel dataset for fine-grained image categorization: Stanford dogs. In *Proc. CVPR workshop on fine-grained visual categorization (FGVC)*, volume 2, 2011.
- Krause, J., Stark, M., Deng, J., and Fei-Fei, L. 3d object representations for fine-grained categorization. In *Proceedings of the IEEE international conference on computer vision workshops*, pp. 554–561, 2013.
- Li, J., Socher, R., and Hoi, S. C. Dividemix: Learning with noisy labels as semi-supervised learning. In *International Conference on Learning Representations*, 2020.

- Li, J., Li, G., Liu, F., and Yu, Y. Neighborhood collective estimation for noisy label identification and correction. *ArXiv*, abs/2208.03207, 2022.
- Li, J., Li, D., Savarese, S., and Hoi, S. Blip-2: Bootstrapping language-image pre-training with frozen image encoders and large language models. In *International conference on machine learning*, pp. 19730–19742. PMLR, 2023.
- Liu, H., Li, C., Li, Y., and Lee, Y. J. Improved baselines with visual instruction tuning. 2024 IEEE/CVF Conference on Computer Vision and Pattern Recognition (CVPR), pp. 26286–26296, 2023.
- Liu, M., Roy, S., Li, W., Zhong, Z., Sebe, N., and Ricci,
   E. Democratizing fine-grained visual recognition with large language models. In *The Twelfth International Conference on Learning Representations*, 2024a.
- Liu, Y., Cai, Y., Jia, Q., Qiu, B., Wang, W., and Pu, N. Novel class discovery for ultra-fine-grained visual categorization. In *Proceedings of the IEEE/CVF Conference* on Computer Vision and Pattern Recognition, pp. 17679– 17688, 2024b.
- Liu, Z., Sun, Z., Zang, Y., Li, W., Zhang, P., Dong, X., Xiong, Y., Lin, D., and Wang, J. Rar: Retrieving and ranking augmented mllms for visual recognition. *arXiv* preprint arXiv:2403.13805, 2024c.
- Maji, S., Rahtu, E., Kannala, J., Blaschko, M. B., and Vedaldi, A. Fine-grained visual classification of aircraft. *ArXiv*, abs/1306.5151, 2013.
- Nilsback, M.-E. and Zisserman, A. Automated flower classification over a large number of classes. In 2008 Sixth Indian conference on computer vision, graphics & image processing, pp. 722–729. IEEE, 2008.
- Parkhi, O. M., Vedaldi, A., Zisserman, A., and Jawahar, C. Cats and dogs. In 2012 IEEE conference on computer vision and pattern recognition, pp. 3498–3505. IEEE, 2012.
- Radford, A., Kim, J. W., Hallacy, C., Ramesh, A., Goh, G., Agarwal, S., Sastry, G., Askell, A., Mishkin, P., Clark, J., Krueger, G., and Sutskever, I. Learning transferable visual models from natural language supervision. In *International Conference on Machine Learning*, 2021.
- Rasheed, H. A., Khattak, M. U., Maaz, M., Khan, S. H., and Khan, F. S. Fine-tuned clip models are efficient video learners. 2023 IEEE/CVF Conference on Computer Vision and Pattern Recognition (CVPR), pp. 6545–6554, 2022.
- Reid, M., Savinov, N., Teplyashin, D., Lepikhin, D., Lillicrap, T., Alayrac, J.-b., Soricut, R., Lazaridou, A., Firat,

- O., Schrittwieser, J., et al. Gemini 1.5: Unlocking multimodal understanding across millions of tokens of context. *arXiv preprint arXiv:2403.05530*, 2024.
- Reimers, N. and Gurevych, I. Sentence-bert: Sentence embeddings using siamese bert-networks. *arXiv* preprint *arXiv*:1908.10084, 2019.
- Ridzuan, M., Bawazir, A., Gollini Navarrete, I., Almakky, I., and Yaqub, M. Self-supervision and multi-task learning: Challenges in fine-grained covid-19 multi-class classification from chest x-rays. In *Annual Conference on Medical Image Understanding and Analysis*, pp. 234–250. Springer, 2022.
- Sohoni, N., Dunnmon, J., Angus, G., Gu, A., and Ré, C. No subclass left behind: Fine-grained robustness in coarsegrained classification problems. In *Advances in Neural Information Processing Systems*, volume 33, pp. 19339– 19352, 2020.
- Touvron, H., Lavril, T., Izacard, G., Martinet, X., Lachaux, M.-A., Lacroix, T., Rozière, B., Goyal, N., Hambro, E., Azhar, F., Rodriguez, A., Joulin, A., Grave, E., and Lample, G. Llama: Open and efficient foundation language models. *ArXiv*, abs/2302.13971, 2023.
- Vaze, S., Han, K., Vedaldi, A., and Zisserman, A. Generalized category discovery. In *IEEE Conference on Computer Vision and Pattern Recognition*, 2022.
- Wah, C., Branson, S., Welinder, P., Perona, P., and Belongie,S. Caltech ucsd bird dataset. Technical Report CNS-TR-2011-001, California Institute of Technology, 2011.
- Wang, P., Bai, S., Tan, S., Wang, S., Fan, Z., Bai, J., Chen, K., Liu, X., Wang, J., Ge, W., Fan, Y., Dang, K., Du, M., Ren, X., Men, R., Liu, D., Zhou, C., Zhou, J., and Lin, J. Qwen2-vl: Enhancing vision-language model's perception of the world at any resolution. arXiv preprint arXiv:2409.12191, 2024.
- Wei, X.-S., Song, Y.-Z., Mac Aodha, O., Wu, J., Peng, Y., Tang, J., Yang, J., and Belongie, S. Fine-grained image analysis with deep learning: A survey. *IEEE transactions on pattern analysis and machine intelligence*, 44:8927–8948, 2021.
- Wolf, T., Debut, L., Sanh, V., Chaumond, J., Delangue, C., Moi, A., Cistac, P., Rault, T., Louf, R., Funtowicz, M., and Brew, J. Huggingface's transformers: State-of-the-art natural language processing. *CoRR*, abs/1910.03771, 2019.
- Yang, G., He, Y., Yang, Y., and Xu, B. Fine-grained image classification for crop disease based on attention mechanism. *Frontiers in Plant Science*, 11:600854, 2020.

- Yang, J., Duan, J., Li, T., Hu, C., Liang, J., and Shi, T. Tool wear monitoring in milling based on fine-grained image classification of machined surface images. *Sensors*, 22 (21), 2022. doi: 10.3390/s22218416.
- Zhou, K., Yang, J., Loy, C. C., and Liu, Z. Learning to prompt for vision-language models. *International Journal of Computer Vision*, 130:2337 2348, 2021.

# **Appendix**

Our code will be made publicly available upon acceptance for further research and reproducibility. This supplementary material contains additional details that we could not include in the main paper due to space constraints, including the following information:

- · Further descriptions of datasets used
- Effect of label filtering on the size of label space
- · Summary of notations and their descriptions
- The overall NeaR algorithm is presented in § A6
- An analysis on an alternative way to obtain candidate sets is shown in § A7.1
- Performance across different prompting strategies in shown in § A7.2
- The impact of varying  $\kappa$ , the number of nearest-neighbors considered is shown in § A7.3
- The effect of choice of threshold  $\tau$  is studied in § A7.4
- Performance across variations in different few-shot splits is shown in § A7.5
- Qualitative Results of NeaR against other baselines in § A7.6
- Discussion on other weaker open-source MLLMs is presented in § A7.7
- Expanded dataset-wise tables due to space constraints in the main paper are presented in § A7.8
- Additional implementation details are given in § A8, where we discuss the hyperparameters of NeaR, present other details of open-source MLLMs, and show the prompts used to generate labels for different MLLMs

**Description of Datasets Used.** We show results on 5 datasets with fine-grained labels – Bird-200, Car-196, Dog-120, Flower-102, Pet-37. In Table A8, we show the number of images used for training and the size of the test set.

	Bird-200	Car-196	Dog-120	Flower-102	Pet-37
Train Set	$m\times 200$	$m\times 196$	$m\times 120$	$m\times 102$	$m \times 37$
Test Set	5794	8041	8550	6149	3669

Table A8: Train and test set sizes of the datasets used in this paper. The number of shots is denoted by m, with m=3 used as the default in our experiments unless otherwise specified.

Method	Average								
	Bird-200	Car-196	Dog-120	Flower-102	Pet-37				
Ground Truths	200	196	120	102	37				
MLLM Labels	412	562	169	183	63				
FineR	202	286	97	112	44				
NeaR-LLaMA	239	305	129	119	45				

Table A9: Label filtering is effective in reducing the size of MLLM generated label to manageable levels.

### Effect of Label Filtering on the Size of Label Space.

As described in § 4.2, label filtering is crucial to obtain good VF-FGVR performance. In Table A9, we present the number of classes in the final classification label spaces that each method operates in. The first row indicates the size of the ground-truth label space. We observe that our label filtering mechanism is essential to combat the openendedness of MLLM labels.

**Summary of Notations.** We represent elements of a set by a subscript and a vector component by a superscript. For instance  $y_i \in \{0,1\}^k$  denotes the one-hot vector encoding of the class label of the *i*-th image,  $i \in [n]$ , and  $y_i^j$  is the *j*-th component of this encoding. Specifically  $y_i^j = 1$  if the *i*-th image is assigned the *j*-th label in the label set  $\mathcal{C}$  and 0 otherwise. A summary of notations is given in Table A10.

# A6. NeaR Algorithm

We present the training algorithm of NeaR in Algorithm 1. We present the three steps of our method NeaR as shown in Figure 1. In lines L1-L7 we generate possibly noisy labels from an MLLM. In lines L8-L12, we then generate a candidate set from  $\kappa$  nearest-neighbors of each image. In lines L19-L27 we train prompt vectors  $\theta$  by minimizing the cross-entropy loss between CLIP predictions and the refined labels. The label refinement in L24 effectively disambiguates the best label from the generated candidates. As training progresses, our estimate of the candidate labels  $q_i$  gets better. The sharpening function is  $\operatorname{shrp}(y,T)^i=(y^i)^{\frac{1}{T}}/\sum_{j=1}^k (y^j)^{\frac{1}{T}}$  and the rescale function is defined as  $\operatorname{rsc}(y,q)^i=(y\odot q)^i/\sum_{i=1}^k (y\odot q)^j$ .

#### A7. Additional Results

In this section we present the following results i) In § A7.1 we analyze an alternative approach to generating candidate sets and compare it with our proposed  $\kappa$ -NN based approach. ii) Different Prompting Strategies like text, visual and both are explored in § A7.2. iii) In § A7.3 we study the impact of varying the number of nearest-neighbors  $\kappa$  on the performance of NeaR; iv) In § A7.4 we study the impact of our

Notation	Description
$egin{array}{c} x_i \ X \ \end{array}$	$i$ -th unlabeled training image set of $n$ training images $\{x_1, x_2, \ldots, x_n\}$ Number of shots of images for each
$l_i = L(x_i, p)$	class belonging to an unknown ground- truth class name set The class label generated for $x_i$ by an
$\mathcal{D} = \{(x_i, l_i)\}_{i=1}^n$	MLLM $L$ with a input prompt $p$ The dataset generated by an MLLM $L$ consisting of image-class name pairs
$C = \bigcup_{i=1}^{n} l_i$ $k =  C $	Label space generated by the MLLM The $k$ lexicographically ordered class names $C = \{c_1, c_2, \dots, c_k\}$
$y_i \in \{0,1\}^k$ $\mathcal{I}$ $\mathcal{T}$ $\theta$	One-hot encoding of the label $l_i$ of $x_i$ Image encoder of pre-trained CLIP Text encoder of pre-trained CLIP Learnable prompt vectors added to the input embeddings of a class name
$f_{\theta}(x) \in \Delta^k$	k-dimensional probability vector of the prompted CLIP model's class predictions for image $x$ , i.e $f_{\theta}(x)^{j} \geq 0$ and $\sum_{i=1}^{k} f_{\theta}(x)^{j} = 1$
$S_i$	Candidate set created by gathering MLLM generated labels of nearest-neighbors of $x_i$
$\mathcal{D}_s = \{(x_i, l_i, S_i)\}_{i=1}^n$	Number of nearest-neighbors Augmented dataset containing the generated label $l_i$ and constructed candidate set $S_i$
$L_{ce}(f_{ heta}(x_i), l_i)$	The cross-entropy loss of CLIP model predictions for image $i$ w.r.t $y_i$ given by $-\sum_{j=1}^k y_i^j log(f_\theta^j(x_i))$ (also written as $L(x_i, l_i)$ )
GMM	A two-component Gaussian Mixture Model fit on loss values of all training samples for every epoch
$w_i = \mathbb{P}_{GMM}(clean x_i)$	The posterior probability of image belonging to the "clean" component, i.e component with lower mean
$ au \in [0,1]$ $X_{cl}, X_{ns}$	Threshold used to partition data into clean and noisy sets  Clean and noisy partitions of the train-
$q_i \in \mathbb{R}^k$	ing data based on $w \ge \tau$ Confidence of the candidates. We have that $q_i^j > 0$ if $c_j \in S_i$ , $q_i^j = 0$ other-
$ar{y}_i$	wise, and $\sum_{j=1}^{k} q_i^j = 1$ Refined label for image <i>i</i> constructed based on whether $x_i$ is clean or noisy.
	For noisy images we rescale the label to have non-zero probabilities only for the candidate labels
$\operatorname{shrp}(y,T)$ and $\operatorname{rsc}(y,q)$	sharpen a distribution $y$ using temperature $T$ ; rescale a distribution $y$ based on candidate confidence $q$
$L_{final}( heta)$ $\mathcal{C}_{test}$	The cross entropy loss between model predictions $f_{\theta}(x)$ and refined labels $\bar{y}$ Inference label space post filtering
test	interested table space post intering

Table A10: List of notations used in our paper, and their descriptions.

#### Algorithm 1 NeaR algorithm: Training **Require:** m-shot training images $X = \{x_i\}_{i=1}^n$ ; MLLM L; input prompt p; number of nearest neighbors $\kappa$ ; CLIP model predictions $f_{\theta}$ with learnable text prompts $\theta$ ; $num\_epochs$ ; $warm\_epochs$ ; learning-rates $\eta$ , $\eta_{warm}$ ; Temperature T**Ensure:** Trained parameters $\hat{\theta}$ Step-1: Labeling training images with an MLLM 1: $D \leftarrow \{\}$ /\* Label each image x by prompting MLLM L with prompt p 2: **for** i = 1, 2, ..., n **do** 3: $D \leftarrow D \cup \{(x_i, l_i := L(x_i, p))\}$ 4: end for 5: $C := \bigcup_{i=1}^{n} l_i$ 6: k := |C|/\* WLOG we consider $C := \{c_1, c_2, \ldots, c_k\}$ where k := $|\mathcal{C}|$ to be lexicographically ordered. Let $y_i$ be the one-hot encoding of label li \*/ 7: $y_i \in \{0, 1\}^k$ and $y_i^j := 1$ if $c_i = l_i$ and 0 o/w **Step-2: Candidate Set Construction** 8: $D_s \leftarrow \{\}$ /\* Augment each image $x_i$ with a candidate set $S_i$ composed of labels of $\kappa$ -nearest neighbors \*/ 9: for $(x_i, l_i)$ in D do 10: $S_i \leftarrow \text{knn\_labels}(x_i, \kappa)$ $D_s \leftarrow D_s \cup \{(x_i, l_i, S_i)\}$ 11: 12: end for $I^*$ We initialize candidate confidence for all images $q_i$ uniformly \*/ 13: $q_i \in \mathbb{R}^k$ and $q_i^j := \frac{1}{|S_i|}$ if $c_j \in S_i$ and 0 o/w Function Partition\_data(D, $f_{\theta}$ , au): $\mathcal{L} := \{ L(f_{\theta}(x_i), l_i) \}_{i=1}^n$ 14: $\mu_c, \sigma_c, \mu_n, \sigma_n \leftarrow fit\_GMM(\mathcal{L})$ 15: $W := \{w_1, w_2, \dots, w_n\}$ where $w_i = \mathbb{P}_{GMM}(clean|x_i)$ $X_{cl} := \{x_i \in X \mid w_i \ge \tau\}$ 16: 17: $X_{ns} := X \setminus X_{cl}$ 18: return $X_{cl}, X_{ns}, W$ Step-3: Fine-tune prompts $\theta$ of a CLIP model 19: **for** $t = 1, 2, ..., num\_epochs$ **do** /\* During warmup, the prompts are tuned on the cross-entropy loss $L_{ce}$ using MLLM generated labels in D \*/if $t \leq warm\_epochs$ then 20: 21:

```
Step-3: Fine-tune prompts \theta of a CLIP model

19: for t=1,2,\ldots,num_epochs do

/* During warmup, the prompts are tuned on the cross-entropy loss L_{ce} using MLLM generated labels in D */

20: if t \leq warm_epochs then

21: \theta_t \leftarrow \theta_{t-1} - \eta_{warm} \nabla L_{ce}(D, f_{\theta_{t-1}})

22: else

/* Every epoch post warm-up, we partition the entire data into clean and noisy sets by fitting a GMM on cross-entropy loss L

*/

23: X_{cl}, X_{ns}, W \leftarrow \text{Partition\_data}(D, f_{\theta_{t-1}}, \tau)

24: \bar{y}_i := \text{shrp}(w_i \cdot y_i + (1 - w_i) \cdot f_{\theta_{t-1}}(x_i), T), if x_i \in X_{cl}
```

/\* We update candidate confidence (for both clean and noisy samples) to be used in the next epoch.  $1[q_i]$  is 1 at non-zero indices and 0 o/w \*/

 $:= \operatorname{rsc}(\operatorname{shrp}(w_i \cdot q_i + (1 - w_i) \cdot f_{\theta_{t-1}}(x_i), T), q_i), \text{ o/w}$ 

```
25: q_{i} \leftarrow \operatorname{rsc}(f_{\theta_{t-1}}(x_{i}), 1[q_{i}])
26: L_{final}(\theta_{t-1}) := \frac{-1}{n} \sum_{i=1}^{n} \sum_{j=1}^{k} \bar{y}_{i}^{j} \cdot \log(f_{\theta_{t-1}}^{j}(x_{i}))
27: \theta_{t} \leftarrow \theta_{t-1} - \eta \nabla L_{final}(\theta_{t-1})
28: end if
29: end for
30: Return: \hat{\theta} = \theta_{num_{enochs}}
```

adaptive thresholding. v) Performance across variations in different few-shot splits is studied in § A7.5. vi) Qualitative results are presented in § A7.6. vii) In S A7.7 we present results on two weaker open-source MLLMs – LLaVA-1.5, and BLIP2; viii) Expanded tables of Comparison of NeaR with JoAPR, PRODEN, on Imbalanced training data and across different backbones in § A7.8.

# A7.1. Analysis on Alternative Ways to Construct Candidate Sets

The labels generated by MLLMs can be noisy. To address this, we propose to construct a candidate set for each image by grouping class labels from the  $\kappa$  nearest-neighbors of the image. In this section we study an alternative approach to candidate set generation, where we query the MLLM itself to generate a set of  $\kappa$  labels directly for each image. We present the results of this approach in Table A11, showing performance across three MLLMs: GPT-40, GeminiPro, and LLaMA.

#### A7.2. Different Prompting Strategies.

We analyze the impact of our proposed approach using various prompting strategies, as presented in Table A12. We consider three distinct prompting methods involving fine-tuning across different modalities: (1) For text-only prompting, we use CoOp (Zhou et al., 2021); (2) For image-only prompting, we employ VPT (Jia et al., 2022); and (3) For both text and image prompting, we adopt hierarchical prompts introduced at different text and image layers (Rasheed et al., 2022) as the backbone. Our method demonstrates strong performance across all prompting strategies, achieving cACC improvements of 4.2%, 1.9%, and 4.1%, respectively. This clearly demonstrates the effectiveness of our method across different fine-tuning methods.

# A7.3. Impact of Varying No. of Nearest-Neighbors $\kappa$

We leverage similarity information to build a candidate set for each image by augmenting its label with the labels of its  $\kappa$  nearest-neighbors. In this section we study the effect of varying  $\kappa$  from 1 to 9 on the performance of NeaR-LLaMA. We perform this experiment for 9-shot data from the Flowers-102 dataset, to ensure that higher values of  $\kappa$  give meaningful results. The results in Figure A3 show that NeaR performs well across a large range of  $\kappa$  values, and justifies our choice of  $\kappa=3$ . Note that setting  $\kappa=1$  is not the same as CoOp-LLaMA, but is the result of NeaR with  $q_i=y_i$ . The results also highlight two competing factors that influence the performance of NeaR as  $\kappa$  varies:

Improved Label Quality with Larger Candidate Sets
 A larger candidate set is more likely to involve a semantically closer label. This is reflected in the upward

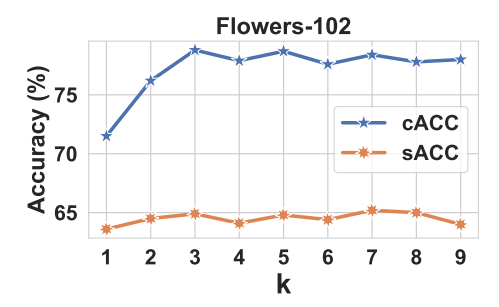


Figure A3: Effect of varying  $\kappa$  (1 to 9) on the performance of NeaR-LLaMA for the 9-shot Flowers-102 dataset. The results show an upward trend in cACC as  $\kappa$  increases from 1 to 3, reflecting an increased likelihood of semantically closer labels. However, for  $\kappa \geq 3$ , the performance plateaus or slightly decreases due to a noisier candidate set, validating our choice of  $\kappa = 3$ .

trend of cACC from  $\kappa = 1$  to  $\kappa = 3$ .

• Increased Noise with Larger Candidate Sets – For higher values of  $\kappa$ , while the likelihood of including better labels in the candidate set increases, it is offset by the addition of irrelevant labels. A noisier candidate set makes it harder for the algorithm to disambiguate the best label in the candidate set. This leads to a plateau or even slight decrease in cACC for  $\kappa > 3$ .

Our proposed approach constructs candidate sets from single labels assigned to each image, while the direct candidate set method generates a set of labels for each image. A notable drawback of the direct approach is the increase in size of the final label space, which may become prohibitively large as each image contributes to  $\kappa-1$  new labels in the worst case. The direct method thus incurs a larger memory footprint and requires longer training times due to the larger label space. For both GPT-40 and GeminiPro, the direct approach termed NeaR-MLLM-Direct encounters an out-of-memory (OOM) error on the Car-196 dataset. Furthermore, for LLaMA, our  $\kappa$ -nn based approach outperforms the direct approach by a substantial margin, achieving a +5.8% higher cACC, while being more efficient.

# A7.4. Effect of Choice of Threshold au

To address the noisy nature of MLLM generated labels, our method NeaR separates samples into clean and noisy sets using a threshold  $\tau$  based on clean posterior probability  $w_i$  of a GMM fitted on loss values. Instead of using a fixed threshold, we make  $\tau$  adaptive by setting it to the mean posterior probability,  $\tau = \frac{1}{n} \sum_{i=1}^{n} w_i$ , allowing dynamic estimation of label noise at every training epoch. We study the effects of using a fixed threshold of  $\tau = 0.5$  for NeaR-LLaMA, NeaR-

Method	Bird-200		Car	-196	Dog	-120	Flowe	er-102	Pet	-37	Ave	rage
	cACC	sACC	cACC	sACC								
NeaR-GPT-4o-Direct NeaR-GPT-4o	53.1 55.8	74.2 75.6	OOM 57.0	OOM 60.0	61.0 61.6	71.9 74.4	77.0 80.6	55.4 52.1	83.1 82.9	82.7 84.0	- 67.6	- 69.2
NeaR-GeminiPro-Direct NeaR-GeminiPro	52.7	73.8 76.0	OOM 54.9	OOM 61.1	70.5 64.7	58.3 75.4	73.9 77.9	46.9 53.2	81.3 79.4	81.7 80.8	66.6	69.3
NeaR-LLaMA-Direct NeaR-LLaMA	43.8 51.0	68.2 70.2	44.7 52.6	56.0 60.9	56.4 59.2	70.6 70.2	70.9 78.6	57.7 61.7	83.2 83.5	87.5 86.2	59.8 <b>65.0</b> (+ <b>5.2</b> %)	68.0 <b>69.8</b> (+1.8%)

Table A11: Evaluation of NeaR-MLLM under different candidate set generation methods. We compare our  $\kappa$ -nn-based candidate set against directly querying the MLLM for a candidate set, referred to as NeaR-MLLM-Direct. For the Car-196 dataset, both GPT-40 and GeminiPro encounter Out-of-Memory (OOM) errors due to the larger label space. For NeaR-LLaMA, our  $\kappa$ -nn-based approach outperforms the direct approach by an average margin of +5.8% in cACC while being more computationally efficient.

Method	Bird-200		Bird-200 Car-196 Dog-120 Flower		er-102	Pet-37		Average				
	cACC	sACC	cACC	sACC	cACC	sACC	cACC	sACC	cACC	sACC	cACC	sACC
	Text Prompting											
CoOp-LLaMA	49.2	68.7	45.5	60.7	58.4	68.4	75.9	59.8	74.4	79.2	60.7	67.4
NeaR-LLaMA	51.0	70.2	52.6	60.9	59.2	70.2	78.6	61.7	83.5	86.2	65.0 (+4.3%)	69.8 (+2.4%)
				Vis	ual Prom	pting						
VPT-LLaMA	48.9	69.5	45.3	61.3	60.3	70.2	78.1	61.7	73.2	82.2	61.1	69.0
NeaR-VPT-LLaMA	50.2	68.5	45.5	60.1	59.4	71.4	78.3	61.3	81.1	84.3	62.9 (+1.8%)	69.1 (+0.1%)
	Multimodal Prompting											
IVLP-LLaMA	48.9	69.5	45.3	61.3	60.3	70.2	78.1	61.7	73.2	82.2	61.1	69.0
NeaR-IVLP-LLaMA	50.8	70.1	52.5	61.0	58.6	69.9	80.3	62.1	83.7	86.4	65.2 (+4.1%)	69.9 (+0.9%)

Table A12: Evaluation of NeaR under different prompting strategies. In addition to text-based prompting, as shown in Tab 3, we present results on Visual Prompting method VPT (Jia et al., 2022) and Multimodal Prompting method IVLP (Rasheed et al., 2022). We outperform the baselines by +1.8% and +4.1% in cACC respectively.

Method	Bird-200		Car	Car-196 Dog-120		-120	Flower-102		Pet-37		Average	
	cACC	sACC	cACC	sACC	cACC	sACC	cACC	sACC	cACC	sACC	cACC	sACC
NeaR-LLaMA ( $\tau$ =0.5)	51.7	70.5	53.3	60.5	59.0	68.6	78.1	61.7	82.2	85.9	64.8	69.5
NeaR-LLaMA	51.0	70.2	52.6	60.9	59.2	70.2	78.6	61.7	83.5	86.2	65.0 (+0.2%)	69.8 (+0.3%)
NeaR-GPT-4ο (τ=0.5)	54.7	74.5	57.9	59.7	62.1	74.6	79.6	52.1	83.0	83.8	67.4	68.9
NeaR-GPT-4o	55.8	75.6	57.0	60.0	61.6	74.4	80.6	52.1	82.9	84.0	67.6 (+0.2%)	69.2 (+0.3%)
NeaR-GeminiPro ( $\tau$ =0.5)	52.8	73.5	53.7	61.1	64.8	75.2	77.6	53.3	77.7	81.0	65.3	68.8
NeaR-GeminiPro	55.9	76.0	54.9	61.1	64.7	75.4	77.9	53.2	79.4	80.8	66.6 (+1.3%)	69.3 (+0.5%)
NeaR-Qwen2 ( $\tau$ =0.5)	34.3	65.0	57.0	64.0	55.2	71.3	74.0	61.4	74.1	76.4	58.9	67.6
NeaR-Qwen2	35.5	65.6	58.0	64.0	56.6	71.7	75.8	62.5	73.8	76.4	60.0 (+1.1%)	68.0 (+0.4%)

Table A13: Evaluation of our dynamic threshold  $\tau$  across different MLLMs compared to a static threshold  $\tau=0.5$ . The use of a dynamic threshold shows consistent improvements across all MLLMs, with gains in NeaR-GeminiPro and NeaR-Qwen2, achieving increases of 1.6% and 1.1% in average cACC, respectively, and a minor gain of 0.2% in other cases. These results support the design choice to avoid the hyperparameter  $\tau$ , which can vary slightly across MLLMs.

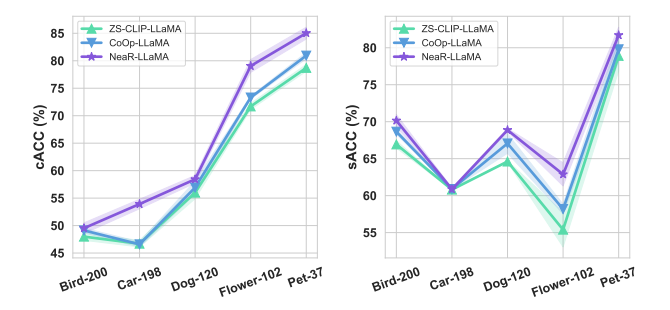


Figure A4: We report cACC and sACC under the effect of random sampling of training images across five datasets. The plot demonstrates minimal variance across datasets, highlighting the robustness of NeaR to variations in data selection.

GPT-40, NeaR-GeminiPro and NeaR-Qwen2 in Table A13. We observe that for NeaR-GeminiPro and NeaR-Qwen2, we have a performance gain of +1.3% and +1.1% in average cACC, while a relatively lower performance gain of +0.2% in NeaR-LLaMA and NeaR-GPT-40. These results show that our adaptive thresholding performs better than a static threshold across a variety of MLLM choices, thus eliminating the need for tuning the hyperparameter  $\tau$ .

# A7.5. Performance across variations in different few-shot splits

We have conducted extensive experiments across three random seeds to evaluate the robustness and consistency of our approach as shown in Fig A4. Specifically, for each seed, we sampled a unique set of m images per class, ensuring diversity in the training data distribution across different runs. The results consistently demonstrate that NeaR outperforms the baseline approaches across various independent samplings, with minimum variance across datasets, indicating its stability and generalizability. This robustness across different random seeds highlights the effectiveness of our approach in handling variations in training data selection, further strengthening its practical applicability in real-world scenarios.

# A7.6. Qualitative Results of NeaR against other baselines.

We visualize a selection of inference images and analyze their predictions across different models. Specifically, we compare the predictions of NeaR against those obtained from directly querying the MLLM, as well as the outputs of ZS-CLIP-LLaMA and CoOp-LLaMA. On the Bird-200 dataset(row 1), NeaR successfully predicts the exact ground-truth label in cases where the MLLM itself fails, demonstrating the effectiveness of our candidate set in guiding classification. Additionally, even in instances where NeaR's

predictions do not match the ground truth, the errors are less severe compared to those of other baselines. For example, for Audi S5 Convertible and Old English Sheepdog, NeaR predicts Audi S5 and English Sheepdog, respectively. While these predictions deviate slightly from the exact ground-truth labels (Audi S5 Coupe and Old English Sheepdog), they remain semantically closer and more reasonable than the mistakes made by other methods.

#### A7.7. Results on Other Open-Source MLLMs

In order to study the impact of NeaR on other opensource MLLMs, we query two weaker open-source MLLMs, LLaVA-1.5 (Liu et al., 2023) and BLIP2 (Li et al., 2023), to generate labels for our datasets. In the context of addressing the VF-FGVR problem, we observe that these models produce generic labels that lack fine-grained detail. For instance, in the Bird-200 dataset, images from various fine-grained classes such as American Goldfinch, Tropical Kingbird, Blue-headed Vireo, Yellow-throated Vireo, Blue-winged Warbler, Canada Warbler, Cape-May Warbler, and Palm Warbler were all labeled simply as 'Bird' by LLaVA. This lack of specificity results in a low cACC of 9.8% for CoOp-LLaVA and 4.7% for NeaR-LLaVA. This trend is also observed with BLIP2. The inability of these MLLMs to generate diverse fine-grained labels makes them a poor choice to solve the VF-FGVR task.

#### A7.8. Expanded Tables

Due to the space constraints in the main paper, we present the detailed dataset-wise results on Comparison of NeaR with contemporary noisy label learning method and partial label learning method in A14, Comparison of NeaR with other baselines under a long-tail class-imbalanced setting in Tab A15 and Comparison of NeaR with baselines across different backbones in shown in Tab A16.

## **A8. Implementation Details**

Apart from the implementation details mentioned in the main paper, we present a few more details. We use a temperature of 2 in the sharpening function. Our batch size is 32. We use the SGD optimizer with a learning rate of 0.002, and use both constant learning rate scheduler and cosine annealing scheduler sequentially. The training hyperparameters are the same for CoOp and NeaR. We sample an equal batch of clean and noisy samples during every epoch. We run all our experiments on a single Nvidia Tesla V100-32GB GPU with an Nvidia driver version of 525.85.12. We use PyTorch 2.4.0 and CUDA 12.0. The default value of number of nearest-neighbors  $\kappa$  is 3, and the number of shots m is 3. We use the few-shot splits provided by FineR (Liu et al., 2024a).



Figure A5: We present qualitative results across five benchmark datasets, comparing predictions from LLaMA, ZS-CLIP-LLaMA, CoOp-LLaMA, and NeaR.

Method	Bird-200		00 Car-196		Dog-120		Flower-102		Pet-37		Average	
	cACC	sACC	cACC	sACC	cACC	sACC	cACC	sACC	cACC	sACC	cACC	sACC
JoAPR-LLaMA	49.2	70.0	42.8	60.6	59.5	70.6	76.7	60.1	73.9	83.3	60.4	68.9
PRODEN	48.3	67.6	45.9	60.6	57.9	67.0	75.2	59.0	75.8	78.5	60.6	66.6
NeaR-LLaMA	51.1	70.2	52.5	60.8	59.2	70.2	78.6	61.7	83.4	86.1	64.9 (+4.3%)	69.8 (+3.2%)

Table A14: Comparison of NeaR with a contemporary noisy label learning method, JoAPR (Guo & Gu, 2024), for CLIP using LLaMA-generated labels. NeaR outperforms JoAPR with an average improvement of +4.6% in cACC and +0.9% in sACC. These results indicate that directly applying LNL methods is insufficient to handle the challenges of noisy MLLM outputs. By incorporating better label refinement using candidate set, and by performing label filtering, NeaR provides a robust solution to the VF-FGVR problem. We also compare our method against PRODEN(Feng et al., 2020). We significantly outperform PRODEN on both cACC and sACC.

Method	Bird-200		Car	-196	Dog	-120	Flowe	er-102	Pet-37		Average	
	cACC	sACC	cACC	sACC	cACC	sACC	cACC	sACC	cACC	sACC	cACC	sACC
FineR	46.2	66.6	48.5	62.9	42.9	61.4	58.5	48.2	63.4	67.0	51.9	61.2
ZS-CLIP-LLaMA	48.9	67.0	46.9	60.3	55.9	64.5	71.4	58.5	75.5	72.2	59.7	64.5
CoOp-LLaMA	47.9	69.9	45.6	60.6	54.2	67.8	74.0	60.2	78.0	74.0	60.0	66.5
NeaR-LLaMA	50.9	69.9	52.6	60.4	60.2	71.2	80.3	63.8	84.6	86.2	65.7 (+5.7%)	70.3 (+3.8%)

Table A15: Performance comparison of NeaR-LLaMA with other baselines under long-tail class distribution. Both NeaR and CoOp retain performance on imbalanced data compared to balanced sampling. NeaR outperforms CoOp by +5.7% in cACC.

Open-Source MLLM details. We utilize the publicly available meta-llama/Llama-3.2-11B-Vision-Instruct model and Qwen/Qwen2-VL-2B-Instruct model from HuggingFace. We observe that instruction tuned MLLMs generate better labels compared to base models. We perform inference using the HuggingFace transformers library (Wolf et al., 2019).

Prompts used to generate labels from MLLMs. In Table A17, we describe the prompts used to obtain the labels for both proprietary and open-source MLLMs. We give different prompts for different datasets. As part of future work, we would like to explore if different prompting strategies can give better labels.

Method	Bird	-200	Car	-196	Dog	-120	Flowe	er-102	Pet	-37	Average	
	cACC	sACC	cACC	sACC	cACC	sACC	cACC	sACC	cACC	sACC	cACC	sACC
RN50												
CoOp-LLaMA	13.9	44.1	8.6	46.6	18.2	47.9	15.6	31.7	36.7	54.7	18.6	45.0
NeaR-LLaMA	17.3	50.5	9.8	48.9	19.9	49.9	20.5	36.6	46.1	63.3	22.7 (+4.1%)	49.8 (+4.8%)
RN101												
CoOp-LLaMA	17.3	45.5	9.6	47.4	20.8	45.4	17.5	34.7	44.0	55.2	21.8	45.6
NeaR-LLaMA	18.6	49.6	11.4	50.8	22.4	51.8	18.9	36.1	47.0	63.9	23.6 (+1.8%)	50.5 (+4.9%)
	ViT-B/16											
CoOp-LLaMA	49.2	68.7	45.5	60.7	58.4	68.4	75.9	59.8	74.4	79.2	60.7	67.4
NeaR-LLaMA	51.0	70.2	52.6	60.9	59.2	70.2	78.6	61.7	83.5	86.2	65.0 (+4.3%)	69.8 (+2.4%)
ViT-B/32												
CoOp-LLaMA	45.0	56.3	39.3	60.5	51.9	66.2	69.8	59.1	72.7	79.8	55.7	66.2
NeaR-LLaMA	48.8	68.4	47.8	60.0	56.4	68.9	75.0	61.3	77.3	82.0	61.1 (+5.4%)	68.1 (+1.9%)

Table A16: Performance comparison of NeaR-LLaMA with CoOp-LLaMA across different CLIP backbones, including ResNet-50 (RN50), ResNet-101 (RN101), and ViT-B/32. For completeness, results are also provided for the default backbone, ViT-B/16. NeaR consistently outperforms CoOp-LLaMA, achieving gains of +4.1% and +4.8% in cACC and sACC for RN50, +1.8% and +4.9% in cACC and sACC for RN101, and +5.4% and +1.9% in cACC and sACC for ViT-B/32.

MLLM	Prompt Structure
GPT-40, GeminiPro	''You are a multimodal AI trained to provide the best fine-grained class label for a given <dataset> image. Provide the best fine-grained class label for the given <dataset> image. Do not return anything else.'', <img/></dataset></dataset>
LLaMA, Qwen	''Give me a fine-grained label for this <dataset>.  For example, <samplelabel>.  Just print the label and nothing else.'', <img/></samplelabel></dataset>

Table A17: A summary of prompts used for querying MLLM models used in this paper. In these prompts,  $dataset \in \{bird, car, dog, flower, pet\}$ . img refers to the image being queried for fine-grained class label. Samplelabel for bird is Black Throated Sunbird, samplelabel for car is 2012 BMW M3 coupe, etc. We observe that open-source models like LLaMA require extra supervision in terms of sample labels for better performance.